Visual servoing of an Earth observation satellite of the LION constellation

Maxime Robic, Renaud Fraisse, Kristen Lagadec, Eric Marchand, François Chaumette

73rd International Astronautical Congress (IAC), Paris, France, 18-22 September 2022.

IAC-22-B1.IP.34.x73936

Visual servoing of an Earth observation satellite of the LION constellation

Maxime Robic[a]*, Renaud Fraisse[b], Kristen Lagadec[c], Eric Marchand[d], François Chaumette[e]

[a] *Inria, Univ Rennes, CNRS, IRISA, Campus de Beaulieu, 35042 Rennes, France*, maxime.robic@inria.fr
[b] *Airbus Defence and Space, 31 Rue des Cosmonautes, 31400 Toulouse, France*, renaud.fraisse@airbus.com
[c] *Airbus Defence and Space, 31 Rue des Cosmonautes, 31400 Toulouse, France*, kristen.lagadec@airbus.com
[d] *Univ Rennes, Inria, CNRS, IRISA, Campus de Beaulieu, 35042 Rennes, France*, eric.marchand@irisa.fr
[e] *Inria, Univ Rennes, CNRS, IRISA, Campus de Beaulieu, 35042 Rennes, France*, francois.chaumette@inria.fr
* Corresponding Author

Abstract

Satellites for observation missions, or imagery satellites, have increased drastically in number and performances since the beginning of the space age. Recent Earth observation satellites are now equipped with new instruments that allow image processing in real-time. Issues such as ground target tracking, moving or not, can now be addressed by controlling precisely the satellite attitude. The satellite "camera" can be used as an input sensor for real-time attitude control process. This can be addressed thanks to a closed loop control scheme that includes the image acquisition and image processing parts. Real-time attitude control using such sensors will then allow the tracking of static or moving ground targets. In this paper, we propose to consider this problem using a visual servoing (VS) approach. This work is thus focused on establishing a visual control law that allows to precisely control a low orbit Earth observation starer satellite attitude using images provided by its matrix sensor. The goal is to perform acquisition missions devoted to gaze on an object of interest that is visible in the image before the VS starts. The visual sensor is fixed to the satellite, and we have full control over its three rotational degrees of freedom subject to dynamic constraints, while the satellite is moving on an orbit that only influences its position (that is not controlled by our VS scheme). Compensating for the target motion in the image by explicitly embedding it in the control scheme becomes essential when it is significant. In our case, the satellite orbit is known, so we can determine accurately its translational motion, and compensate for it in the control law. When it comes to target motion, we propose to decompose it into a known displacement caused by Earth's dynamics and a residual motion due to its potential own motion. The contribution of this paper is a visual servoing scheme able to control the attitude of an agile Earth observation satellite for target tracking. Three visual features are selected for controlling the 3 attitude parameters, for achieving a centering task, and an orientation task. The control law allows for dealing with the satellite's high translational velocity induced by its orbit and other external motion including Earth's rotation and target own motion. A rate saturation algorithm is also proposed dealing with dynamic constraints. Simulations and experiments on an actual robot will be presented.
Keywords: visual servoing, earth observation satellite, target tracking.

Acronyms/Abbreviations

Visual servoing (VS), Image-based visual servoing (IBVS), Degrees of Freedom (DoF).

1. Introduction

Earth-pointing satellites for observation missions, or imagery satellites, have increased drastically in number and performances since the beginning of the space age. For example, Pléiades HR, a constellation of two imagery satellites on a sun-synchronous quasi-circular orbit at 695km, acquires Earth image with 70cm of resolution [1]. Pléiades image acquisition system uses push-broom technology (see Fig. 1), i.e., a sensor line allows to scan a 20km image swath (line by line acquisition) to cover both Defense and civilian observation needs. The Pléiades Néo constellation [2] aims to ensure the continuity and improve the current system in terms of satellite capability and acquisition resolution. To perform an acquisition mission, a desired satellite attitude is maintained thanks to an on-board attitude controller [3]. However, the attitude guidance is not modified in real-time, i.e., the requested attitude is programmed before the acquisition. Still, real-time attitude adjustments might have relevant interest for ground targeting (e.g., to track a moving target in real-time, or to improve the 3D reconstruction of Earth surface using satellite images [4], ...).

A motionless ground target tracking approach using a real-time control loop is studied in [5]. The tracking error is regulated using a model predictive control approach based on the satellite dynamics. Yet, the target is considered fixed on the Earth and the image acquisition is only considered as an output, as push-broom technologies are not compatible with real-time video image processing and control. Airbus Defence & Space is developing a new satellite system with a "Starer" acquisition principle (see Fig. 1). The acquisition is performed by a matrix of sensors that allows real-time

acquisition of the images (2D image acquisition at once) and thus video of a target area. This way, the satellite "camera" could be used as an input sensor for real-time attitude control. Airbus DS plans to embed this new technology into the future LION constellation composed of several agile Earth observation satellites acquiring images of 50-cm resolution at a 5-Hz frequency. Real-time attitude control using such sensors will then allow the tracking of motionless and moving ground targets. In this paper, we show that this precise control of the satellite could be achieved using a closed loop visual servoing (VS) control scheme [6].

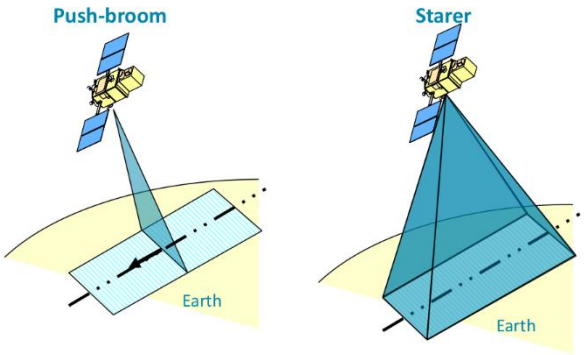

Figure 1:Push-broom and starer technologies

Visual servoing is widely used for space applications as it provides autonomous and efficient control for solving precision tasks, with real-time pose adjustments. Space Rendezvous has been considered in [7] using 3D model-based tracking together with a 2 1/2 D visual servoing control law. Satellite capture has also been studied [8,9] with various image-based visual servoing control laws for free-floating space manipulators. In these works, the target is either considered to have a known motion [9] or an unknown motion [8]. In [10], a visual servoing of a multi-arm system is performed to improve on-orbit servicing by combining visual servoing with other robotic tasks to reduce attitude disturbance. Finally, another image-based control process for observing tumbling objects has been studied in [11].

The main difference between these studies and our application is that they do not have to deal with large velocity difference between the target and the sensor. Indeed, for the above works, the two considered objects are moving in almost the same orbit, which is not the case for our application, while the orbital velocity of the satellite is one of the main issues for solving the tracking problem.

This work is focused on establishing a visual control law that would allow to precisely control a LION satellite attitude using images provided by the starer sensor. The goal is to perform acquisition missions devoted to gaze on an object of interest (see Fig. 2). The sensor is fixed to the satellite that is supposed to move on a sun-synchronous circular orbit at 500km altitude. We have full control over the three rotational DoF of the satellite subject to dynamic constraints, while the satellite orbit only influences its position (that is not controlled by our VS scheme).

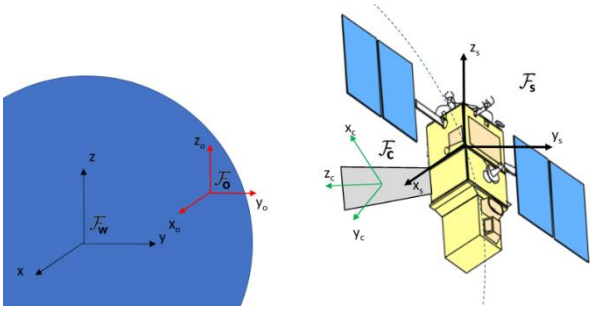

Figure 2: LION mission: a satellite (Fs) directed by its orbital translation and controlled in rotation to track a terrestrial object of interest (Fo) thanks to its camera (Fc). World frame (Fw) is here the equatorial geocentric frame of reference.

We suppose that the target is visible in the image before the VS starts. Furthermore, any previous motion to orientate the satellite roughly toward a requested area is done by an open-loop attitude guidance law. Compensating the system dynamics [12,13,14] by explicitly including it in the control scheme becomes essential when its own motion is significant. In our case, the orbit of the satellite is known, so we can estimate accurately its translation motion, and compensate for it in the control law. When it comes to target motion, various approaches exist in the literature [15]. We propose to decompose the target motion into a known displacement caused by the Earth's dynamics and a residual motion due to the target own motion.

The contribution of this paper is a visual servoing scheme capable of controlling the attitude of an agile Earth observation satellite for target tracking. The control law allows to deal with the satellite's high translational velocity induced by its orbit and other external motion including Earth's rotation and target own motion. A predictive rates saturation algorithm is also proposed for dealing with the dynamic constraints of the satellite.

2. Theory and calculation

2.1 System overview

The VS loop is presented in Fig. 3. The target is first selected into the image, from which desired visual features are set for specifying the task to be achieved. Angular rates are computed by image-based visual servoing, then subject to a predictive saturator, which potentially limits the computed rates, before being fed to the low-level controller that manages the satellite attitude

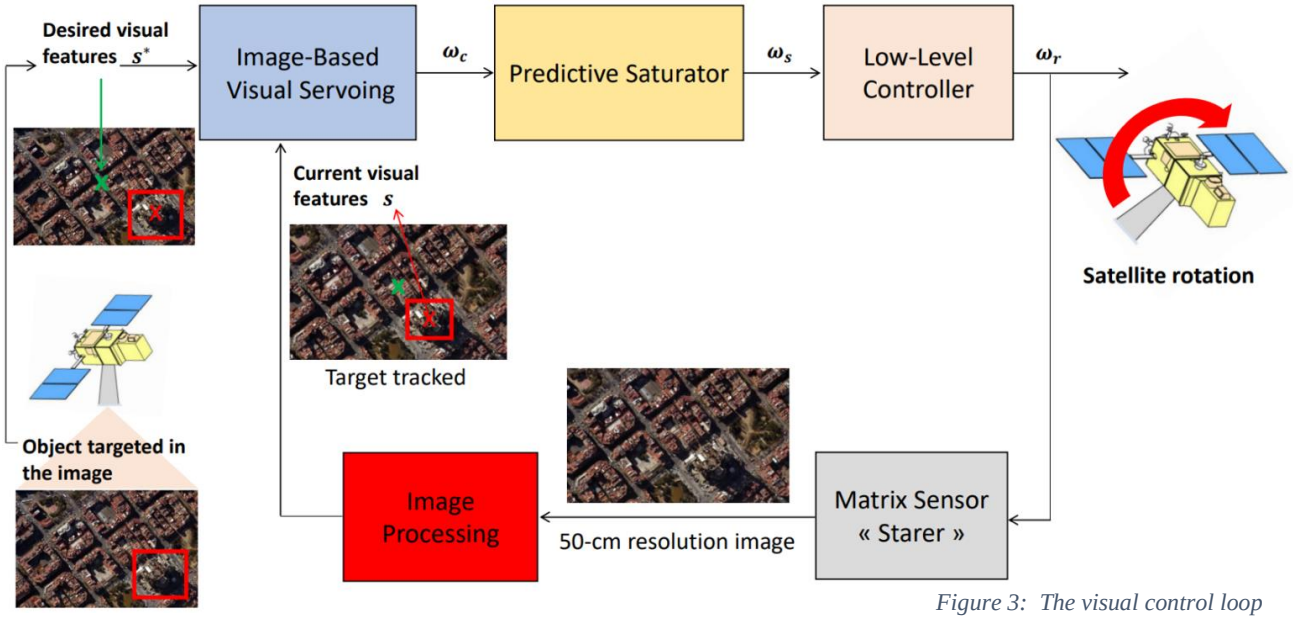

Figure 3: The visual control loop

dynamics and control. Image processing tracks the target in the image acquired by the matrix sensor, and updates the current visual features, from which a new iteration of the loop is performed**.**

2.2 Visual servoing

The closed-loop attitude control is based on a visual servoing scheme designed to track an object of interest through image flow and to guarantee a straight-line trajectory of the target in the image if it is static on the Earth. The full study of the proposed VS scheme has been done in [16]. The angular rates computed by the image-based VS step is expressed by:

$$\boldsymbol{\omega_c} = -\boldsymbol{L}^{+}_{\boldsymbol{\omega_c}}\left(\boldsymbol{\Lambda e} - \boldsymbol{L_s}\left({}^{c}\boldsymbol{v}_s - {}^{c}\boldsymbol{v}_{o_E}\right) + \mu \textstyle\sum_j \boldsymbol{e}(j)\right) \quad (1)$$

which is computed at a 5-Hz frequency. Let us define each term above:

- **e** is the visual error function to be regulated to 0. It is expressed by:

$$\mathbf{e} = \boldsymbol{s} - \boldsymbol{s}^* \quad (2)$$

with $\boldsymbol{s}$ and $\boldsymbol{s}^*$ respectively the current and the desired visual features, that are expressed by:

$$\boldsymbol{s} = \begin{pmatrix} x \\ y \\ \alpha \end{pmatrix}, \ \boldsymbol{s}^* = \begin{pmatrix} x^* \\ y^* \\ \alpha^* \end{pmatrix} \quad (3)$$

where (x, y) is the image coordinates of a point **P** belonging to the targeted object, typically its center of gravity, and (x^*, y^*) is the desired image position of the target. These two visual features allow achieving a centering task. Then, another point **P'** of the target is considered to compute the target orientation α in the image. The visual feature α is defined as $arctan\frac{y-y'}{x-x'}$, that is the angle of $[\boldsymbol{x}, \boldsymbol{x}']$, the projected segment **[P, P′]** onto the image plane with the horizontal axis, and α^* is

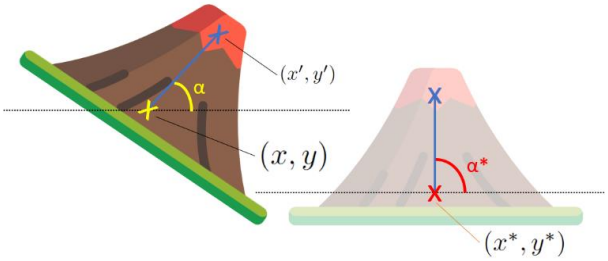

Figure 4: The three visual features defining the centering and the orientation tasks

its desired value (see Fig. 4). This third visual feature allow achieving an orientation task.

For instance, to obtain images centered on the target, we set $x^* = y^* = 0$. Additionally, to observe the sky on the top and the ground on the bottom, the second point **P'** is selected above the target, i.e., with a different altitude, and the corresponding segment **[P, P′]** must appear as vertical in the image, in which case $\alpha^* = \frac{\pi}{2}$.

-**Λ** is a proportional gains matrix, expressed by:

$$\boldsymbol{\Lambda} = \begin{pmatrix} \lambda & 0 & 0 \\ 0 & \lambda & 0 \\ 0 & 0 & \lambda_\alpha \end{pmatrix} \quad (4)$$

where each gain λ is adaptive (error-dependent), which means they are modulated to decrease high velocities when the visual error is high (low value of λ), and increase convergence speed when it is low (high value of λ) [16]. The angular rate around the *z*-axis is decoupled from *x* and *y* axes because limitations on yaw are stricter than on roll and pitch (see Section 2.3).

-$\boldsymbol{L}_{\boldsymbol{\omega}_c}^{+}$ is the inverse of the 3x3 image Jacobian $\boldsymbol{L}_{\boldsymbol{\omega}_c}$ related to the visual error whose full expression is given by:

$$\boldsymbol{L}_{\boldsymbol{\omega}_c} = \begin{pmatrix} xy & -1-x^2 & y \\ 1+y^2 & -xy & -x \\ -xs^2 & -yc^2+xcs & -1 \end{pmatrix} \quad (5)$$

where $s = \sin\alpha$ and $c = \cos\alpha$.

- ${}^{c}\boldsymbol{v}_{s}$ is the satellite's translational velocity (order of magnitude 7 km/s) expressed in camera frame F_c (see Fig. 2) induced by orbital motion, whose expression is known and computable by orbital mechanics.

- ${}^{c}\boldsymbol{v}_{o_F}$ is the target's translational velocity induced by Earth's rotation (order of magnitude 0.4 km/s at equator) expressed in camera frame F_c, whose expression is also known and computable by orbital mechanics.

-$\boldsymbol{L}_s$ is the 3x3 image Jacobian related to translational velocities induced by satellite and Earth's dynamics. It is expressed by:

$$\boldsymbol{L}_s = \begin{pmatrix} \frac{-1}{Z} & 0 & \frac{x}{Z} \\ 0 & -\frac{1}{Z} & \frac{y}{Z} \\ -\frac{d}{l}s & \frac{d}{l}c & \frac{d}{l}(xs-yc) \end{pmatrix} \quad (6)$$

with $l = \sqrt{(x-x')^2+(y-y')^2}$ the length of the segment $[\boldsymbol{x}, \boldsymbol{x}']$ on the image plane and *d=1/Z'–1/Z* with *Z* and *Z'* respectively the depth of **P** and **P'**. This expression cannot be used when l is nearly null (which occurs when the satellite is close to the zenith of the target) since the visual feature α is not well-defined in that case. In this situation, the orientation task cannot be performed and the visual feature α is disabled from the visual error **e**, which implies the dimension of matrices $\boldsymbol{L}_{\boldsymbol{\omega}_c}$ and $\boldsymbol{L}_s$ are now 2x3. They are expressed by:

$$\boldsymbol{L}_{\boldsymbol{\omega}_c} = \begin{pmatrix} xy & -1-x^2 & y \\ 1+y^2 & -xy & -x \end{pmatrix},\ \boldsymbol{L}_s = \begin{pmatrix} \frac{-1}{Z} & 0 & \frac{x}{Z} \\ 0 & -\frac{1}{Z} & \frac{y}{Z} \end{pmatrix} \quad (7)$$

and $\boldsymbol{L}_{\boldsymbol{\omega}_c}^{+}$ is now the Moore-Penrose pseudo-inverse of $\boldsymbol{L}_{\boldsymbol{\omega}_c}$.

-$\mu\sum_j \boldsymbol{e}(j)$ is an integrator. When the target has its own unknown motion, this motion, unlike previous translational velocities, cannot be injected in the control scheme. The integrator will eventually eliminate the tracking error induced by a constant motion in the image. μ is the integral gain, which is also adaptive and must be tuned to allow for a smooth compensation of the tracking error.

2.3. Predictive saturator

Due to mechanical and security reasons, the dynamics of the satellite is limited to a certain maximum:

- on the *x* and *y* axes, i.e., for roll and pitch, the angular rate is limited to 3 deg/s and acceleration to 0.6 deg/s²,
- on the *z* axis, i.e., for yaw, the angular rate is limited to 1.2 deg/s and acceleration to 0.25 deg/s².

To ensure that these limits will not be exceeded, a predictive saturator has been designed from the known dynamics response of the satellite to the low-level attitude controller. The Laplace transfer function of this response is given by:

$$F(p) = \frac{2z_c\omega_0 p+\omega_0^2}{p^2+2z_c\omega_0 p+\omega_0^2} \quad (8)$$

whose coefficients ($z_c = \frac{\sqrt{2}}{2}$ and $\omega_0 = \pi$) induce a pseudo-periodic regime that triggers a latency (~2s) in the execution of the computed angular rates. Thanks to the knowledge of this transfer function, it is possible to predict what would be the effect of a sending a new $\boldsymbol{\omega}_c$ at each iteration of the VS loop. We denote $\boldsymbol{\omega}_p$ the prediction of the rates $\boldsymbol{\omega}_r$ actually operated by the satellite. It is given by:

$$\boldsymbol{\omega}_p(t) = \sum_{i=0}^{k}[(\boldsymbol{\omega}_c(i)-\boldsymbol{\omega}_c(i-1)) * (f(t-i*dt) - f(t-(i+1)*dt))] + \boldsymbol{\omega}_r(t-dt) \quad (9)$$

where $\boldsymbol{\omega}_c(i)$ is the angular rates computed by VS at iteration i at a 5-Hz frequency (so $dt = 200ms$), k is the length of the considered time window (k~10), and $f(t)$ is the time response of the low-level controller for a unit step directly obtained from (8):

$$f(t) = (1 - e^{-z_c\omega_0 t}(\cos(z_c\omega_0 t) - \sin(z_c\omega_0 t)) \quad (10)$$

Thanks to $\boldsymbol{\omega}_p$, it is possible to detect if a limit would be exceeded and to determine a $\boldsymbol{\omega}_s$ so that it does not occur.

A saturation algorithm is thus applied by considering each component ω_{pi} of $\boldsymbol{\omega}_p$ given by (9). When a limit is detected, a reduction factor is computed on the axis concerned. Reduction factors $(r_x^{\gamma}, r_y^{\gamma}, r_z^{\gamma})$ for instant acceleration constraints and $(r_x^{\omega}, r_y^{\omega}, r_z^{\omega})$ for angular rates constraints are computed according to the following rules:

- $\forall i \in [x,y,z]$ if $|\gamma_i| > \gamma_{max_i}$ where $\gamma_i = \frac{\omega_{pi}(t)-\omega_{ri}(t-dt)}{dt}$ then $r_i^{\gamma} = \frac{\gamma_{max_i}}{|\gamma_i|}$ else $r_i^{\gamma} = 1$.
- $\forall i \in [x,y,z]$ if $|\omega_{pi}| > \omega_{max_i}$ then $r_i^{\omega} = \frac{\omega_{max_i}}{|\omega_{pi}|}$ else $r_i^{\omega} = 1$.

Then, as the *z*-axis has different constraints than the others, and for not penalizing the time-to-convergence of the centering task, we adopt the following strategy:

- exceeding velocity or acceleration constraints on *x* or *y* axis induces a velocity reduction on all axes i.e., $r_x = r_y = r_z$,
- exceeding constraints on z axis induces a velocity reduction on *z* axis only, i.e., $r_x = r_y = 1$.

- exceeding constraints simultaneously on multiple axes induces that $r_x = r_y = \min(r_x, r_y)$ and $r_z = \min(r_x, r_y, r_z)$.

This strategy has been designed to perturb as few as possible the straight-line trajectory of the target in the image in case it is static on the Earth.

Finally, when an acceleration constraint is breached, the angular rates $\boldsymbol{\omega}_s$ sent to the low-level controller is given by:

$$\boldsymbol{\omega}_s(t) = \frac{\boldsymbol{R}^{\gamma}\left(\boldsymbol{\omega}_p(t) - \boldsymbol{\omega}_r(t-dt)\right) - \sum_{i=0}^{k-1} \boldsymbol{g}(i)}{f(dt)} + \boldsymbol{\omega}_s(t-dt) \qquad (11)$$

where:

- $\boldsymbol{R}^{\gamma} = \begin{pmatrix} r_{xy}^{\gamma} & 0 & 0 \\ 0 & r_{xy}^{\gamma} & 0 \\ 0 & 0 & r_z^{\gamma} \end{pmatrix}$,
- $\boldsymbol{g}(i) = \left(\boldsymbol{\omega}_c(i) - \boldsymbol{\omega}_c(i-1)\right) * \left(f(t - i * dt) - f(t - (i+1) * dt)\right)$.

Note that $\boldsymbol{\omega}_s = \boldsymbol{\omega}_c$ if $\boldsymbol{R}^{\gamma} = \boldsymbol{I}_3$. The above formula ensures that the actual angular acceleration of the satellite will not exceed its limits.

Then, if $\boldsymbol{R}^{\gamma} \neq \boldsymbol{I}_3$, a new prediction $\boldsymbol{\omega}_p$ must be computed with $\boldsymbol{\omega}_s$ in (9) to test if the new prediction exceeds the angular rates constraints.

Finally, if angular rates constraints are breached, we set:

$$\boldsymbol{\omega}_s(t) = \frac{\boldsymbol{R}^{\omega}\boldsymbol{\omega}_p(t) - \boldsymbol{\omega}_r(t-dt) - \sum_{i=0}^{k-1} \boldsymbol{g}(i)}{f(dt)} + \boldsymbol{\omega}_s(t-dt) \qquad (12)$$

where $\boldsymbol{R}^{\omega} = \begin{pmatrix} r_{xy}^{\omega} & 0 & 0 \\ 0 & r_{xy}^{\omega} & 0 \\ 0 & 0 & r_z^{\omega} \end{pmatrix}$.

At the end, we have $\boldsymbol{\omega}_s = \boldsymbol{\omega}_c$ if $\boldsymbol{R}^{\omega} = \boldsymbol{R}^{\gamma} = \boldsymbol{I}_3$ (that is, no limit has been detected), and our saturation algorithm guarantees that each $\boldsymbol{\omega}_s$ sent to the low-level controller implies $\boldsymbol{\omega}_r$ to ensure the satellite dynamic constraints.

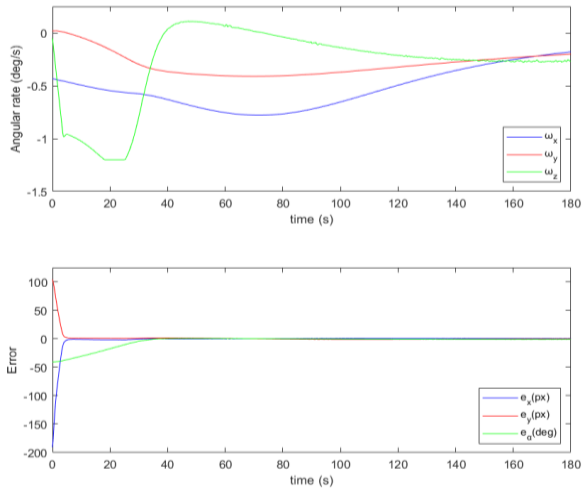

Figure 5: Measured angular rate $\boldsymbol{\omega}_r$ and visual feature error for the visual control law applied for satellite simulation flying over the port of Brest.

3. Results and Discussion

The proposed control law was tested using the ViSP framework [17]. To achieve a realistic experiment, we

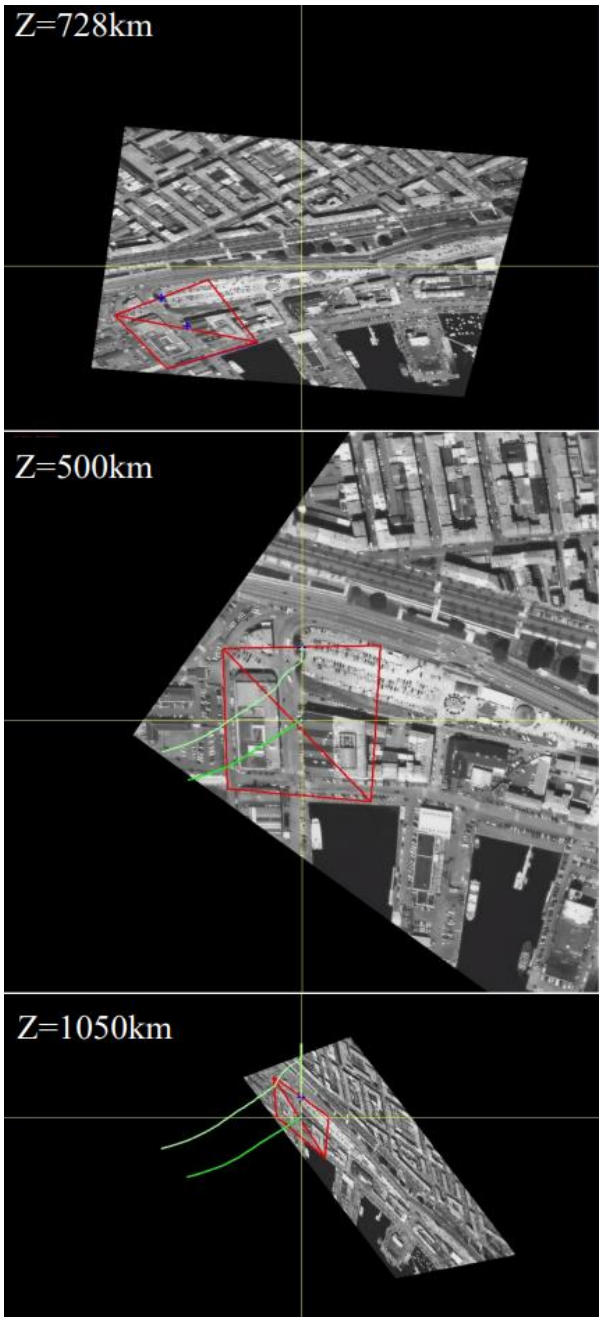

Figure 6: Image trajectory of point $\boldsymbol{P}$ and $\boldsymbol{P}'$ induced by visual control law in satellite simulation targeting an object of interest in the port of Brest. Satellite motion can be observed as it gets closer to the target, distance to target is reduced from 730km to 500km and both the image and the template are enlarged. After reaching zenith, the satellite moves away. The distance to target increases and the image and the template shrink.

have first considered the simulation of the trajectory of a sun-synchronous satellite flying over real scaled satellite images and performing visual servoing to center a terrestrial object of interest in the image. Then, the tracking of fast-moving targets has also been considered with full simulation of the visual features (without real images). Finally, our control law has been applied to a Cartesian robot performing a downscaled satellite movement in various configurations.

In all cases, the visual loop starts when the object of interest is in the camera field of view. We consider that the satellite is already pointing on an area of interest containing the target using an open-loop attitude controller that compensates the satellite and Earth motions. This controller achieves the following angular rates:

$$\boldsymbol{\omega}_r(t) = \boldsymbol{L}_{\omega_c}^{+}\boldsymbol{L}_s\,({}^c\boldsymbol{v}_s(t) - {}^c\boldsymbol{v}_{o_E}(t)) \qquad (14)$$

and we initialize the very first angular rates of the visual loop with the value $\boldsymbol{\omega}_r(t_0)$ at its initial time t_0.

3.1 Satellite simulation

In this section, we simulate an actual satellite and its dynamics, moving in a sun-synchronous circular orbit at 500km altitude, targeting a terrestrial target, motionless or not. The control loop is synchronized with the camera frequency embedded on the satellite, which is 5Hz. Visual features are either measured within real images or simulated ones.

3.1.1 Real images for static target tracking

A 50cm-resolution image of the port of Brest (France) has been used to perform a simulated acquisition close to reality. The distance to the target is computed thanks to the knowledge of the satellite trajectory and the known longitude and latitude of the area of interest. An initial template is selected manually (object detection is not in the scope of this paper). It is then tracked by computing a homography using a SSD inverse compositional template tracker [18]. The center of the reference zone is the target and the center of the top boundary of the reference zone is the second point of the image segment from which angle α is computed. Fig. 6 shows different images acquired during the satellite motion induced by its orbital translations and its rotations induced by the visual control law. As expected, the image trajectory of the target while performing the centering task is a straight line in the image, and the control scheme succeeds in keeping the target at the center of the image with the desired orientation, in spite of satellite translations. From Fig. 5, we can see that the centering task converges very fast (in less than 5 seconds) while the orientation task is achieved more slowly (in 30 seconds approximatively). This is due to the large initial error of α and the stricter constraints on the yaw axis whose acceleration is saturated at the beginning and whose angular rate is then saturated from approximatively 15 to 25 seconds.

3.1.2 Tracking fast-moving targets

To evaluate the tracking efficiency for moving targets, a simplified control scheme considering only the centering task is operated on simulated terrestrial targets. Targets are assumed to move with a fast constant velocity, and an integrator is set in the control loop to compensate for the tracking error induced by this motion. We can observe in Fig. 7 the large effect of the target motion: for the first segment that corresponds to the first iteration of the control scheme, i.e., until t=0.2s, the visual servo has no effect due to the latency of the satellite attitude dynamics and control. The influence of

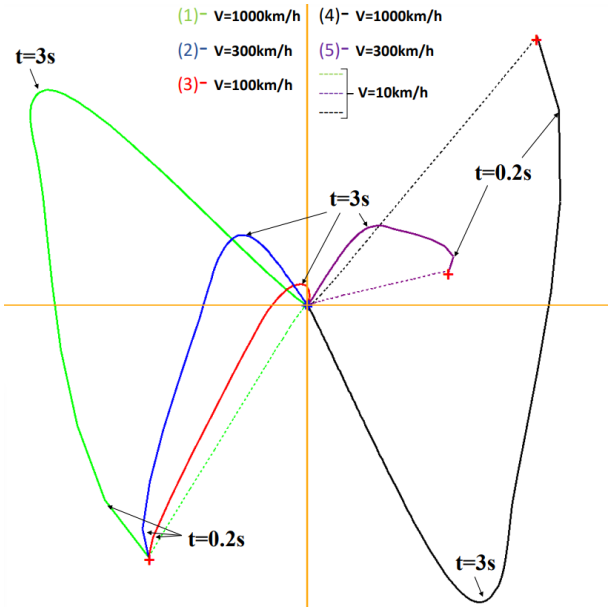

Figure 7: Image trajectory of mobile targets with different configurations. Targets (1), (2) and (3) are starting from the same origin and moves with the same direction, and they are respectively moving at a constant speed of 1000km/h, 300 km/h and 100 km/h. Targets (4) and (5) are respectively moving at a constant speed of 1000km/h and 300km/h, but with different origins and directions. Dotted curves are image trajectories of the mobile targets if their speed was very low (10km/h).

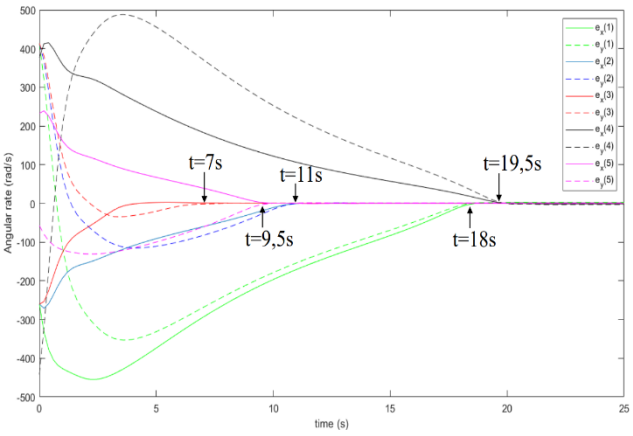

Figure 8: Visual feature error during the tracking of fast-moving targets in different configurations.

this latency is visible until t=3s on visual errors and on the target point trajectory. The bend that is present on each curve at t=3s would be almost the final position of the target in the image if there was no integrator in the control loop. It is clear that the tracking error amplitude varies according to the target speed. Finally, from t=3s, we can see a greater influence of the integrator that finally reduces and cancels the tracking error. In Fig. 8 we can notice the time-to-convergence where all the residual error is totally eliminated for each configuration. As the integrator gain μ is tuned to achieve a smooth compensation of the tracking error, this time-to-convergence is directly dependent of the value of the target speed. This use case shows that any terrestrial object that moves at a constant speed can eventually be tracked and centered by our control law, as long as the target does not move away from the image at the beginning when visual servoing effect is reduced by the latency of the satellite dynamics and when the integrator has no influences yet.

3.2 Implementation on a Cartesian robot

The control law has also been implemented on a Cartesian robot performing a downscaled satellite movement. The robot is a 6 DoF Gantry robot. Its end-effector is equipped with a camera mounted with a pan-tilt configuration (see Fig. 9).

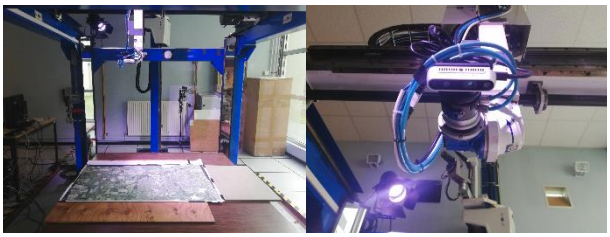

Figure 9: Experimental setup: a satellite image positioned below a Cartesian robot and the Intel D435 camera with a pan-tilt configuration.

The robot moves with a downscaled satellite trajectory while the camera attitude is controlled by visual servoing. As in previous sections, the robot is also simulating the dynamic behavior of the satellite. The camera is pointing at a scaled satellite image reflecting our application scenario. Three configurations are presented in Fig. 10: a planar configuration where two points determine the desired orientation (the two points have the same altitude), a configuration with relief (where the two points share the same longitude and latitude but have different altitudes) and a moving object configuration (where we only consider the centering task). The robot is moving in translation with a typical satellite trajectory whose translational velocities are reduced by a factor S_c related to the ratio between the altitude of the simulated satellite, which is fixed at 1 meter, and the real one, which is 500km at the zenith ($S_c = 2 \times 10^{-6}$). Additionally, the depth Z of the target is fixed at 1 meter for every configuration and for any camera inclination.

3.2.1 Planar configuration

In the planar configuration, the two points defining the centering and the orientation tasks are at the same altitude. In Fig. 10 (left), we can see that the control law succeeds in centering the target with almost a perfect straight-line trajectory, and finally orientating it without deviation from the center. The influences of our saturation algorithm can be seen in Fig, 11 (left). Indeed, at the beginning, the *y*-axis acceleration is saturated (linear decrease of ω_y with a slope of a_{max_y}) that makes *x* and *z* axes saturated as well but with different slopes, as defined in Section 2.3. In the image trajectory, it is observed by a slight bending of the curve at the beginning. Then, when the centering task is completed, the speed of the *z*-axis is saturated (constant ω_{max_z}) as the adaptive gain λ_α is tuned to complete the orientation task as fast as possible without altering the nature of the straight-line trajectory. Finally, when both tasks have converged, the control law succeeds in compensating for the robot translational motion, keeping the visual features errors low.

3.2.2 Configuration with relief

In the configuration with relief, the two points defining the centering and the orientation task have the same longitude and latitude but a different altitude. To do so (see Fig. 11 middle) the template tracking is operated on a picture of the Eiffel tower set out of the plane. In this configuration, the satellite is flying over the scene without passing through the zenith of the target, so that, as explained in Section 2.2, the angle α is always well-defined. As in the previous configuration, the control scheme converges with a straight-line trajectory of the target, and then the orientation task is completed. The same observations on saturation as in the planar configuration can be made: acceleration saturation of *x*-axis at the beginning then rate saturation of *z*-axis without altering the straight-line trajectory.

3.2.3 Moving target configuration

In this last situation, only the centering task is considered to track a moving car with an almost constant speed (see Fig. 10 right). As in previous experiments, the target first moves in the image to a position with a tracking error since the integrator has almost no influence at the beginning of the servoing process (see Fig. 11 right). Then, the integrator has more influence and smoothly compensates for the tracking error. During the compensation of the residual error, angular rates are slightly oscillating because the template tracking is operated on a small area, which makes it difficult to be tracked, and because the speed of the vehicle is not perfectly constant as it is manually displaced.

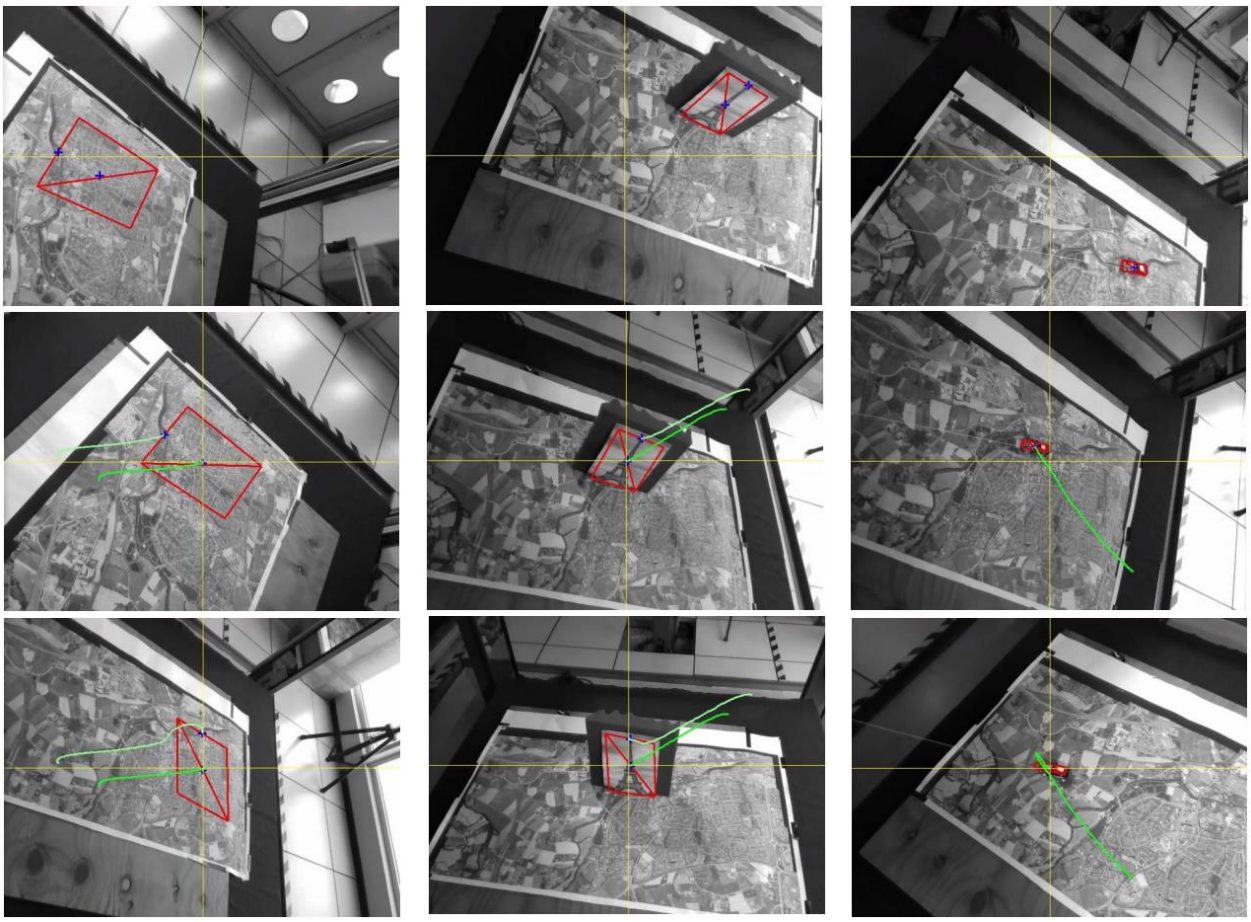

Figure 10: image trajectory of point P and P' induced by visual control law in plane (on the left), relief (on the middle) and moving target (on the right) configurations: at the beginning (on the top), when centering errors are low (on the middle), and at the end (on the bottom). In the two first situations, a straight-line trajectory is observed while completing the centering task, then the target is kept on the center of the image while the orientation task ends. In the last configuration, a straight-line trajectory happens while reaching the original position of the car, then during the compensation of the tracking error induced by its motion.

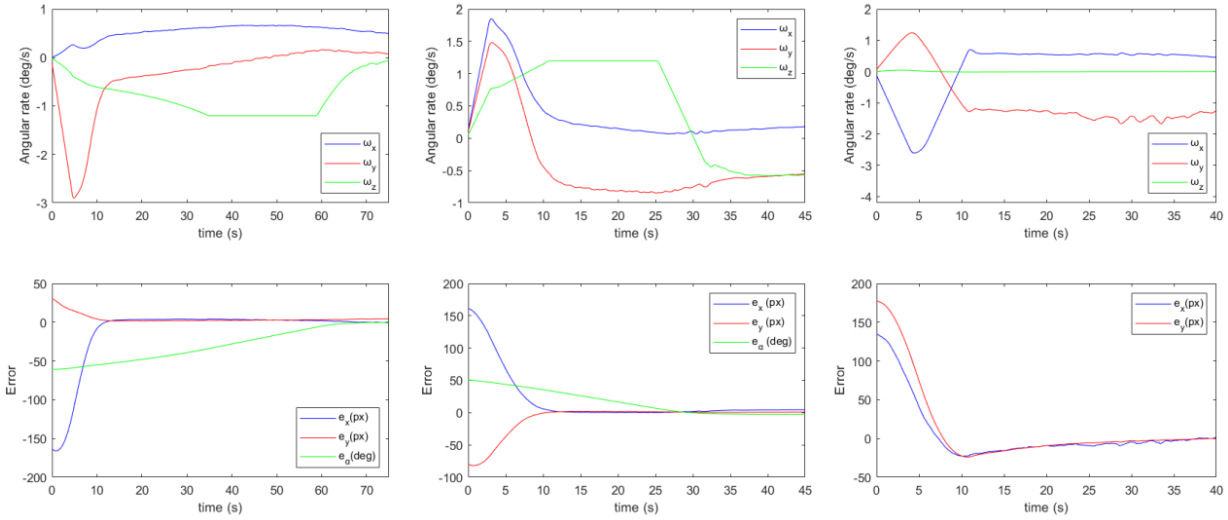

Figure 11: Measured angular rate $\boldsymbol{\omega}_r$ and visual feature error for the visual control law in plane (on the left), relief (on the middle) and moving target (on the right) configurations.

Nevertheless, the control scheme succeeds in tracking the car in the image despite the car's own motion and the robot translational velocity.

In each situation, the control law succeeds in compensating for the robot translational motion and in minimizing the visual feature errors (see Figs. 10 and 11). These results are similar with those obtained on satellite simulation, as the nature of the trajectory is the same, order of magnitude of the error and of the angular rates are similar. Finally, the visual servoing scheme succeeds in converging for all configurations presented here.

4. Conclusions

In this paper, a visual servoing scheme has been proposed to control precisely the full attitude of a low-orbit Earth observation satellite, aiming to target terrestrial objects on the Earth's surface. A new control law has been developed while taking into account translational velocity of the satellite induced by its orbit, possible target own speed, angular rate constraints and satellite dynamics. Our image-based controller has been evaluated on a Cartesian robot simulating a downscaled satellite movement and realistic images acquisition. Simulations with real images have also been considered. The results demonstrated the ability to track any terrestrial object, motionless or with low or high constant velocity.

Acknowledgements

This work was supported by BPI France Lichie project.

References

[1] M. A. Gleyzes, L. Perret, and P. Kubik. Pleiades system architecture and main performances. *Int. Archives of the Photogrammetry, Remote Sensing and Spatial Information Sciences*, 39(1):537–542, 2012.

[2] J. Soubirane. Shaping the future of earth observation with Pléiades neo. In *2019 9th International Conference on Recent Advances in Space Technologies* (RAST), pages 399–401, 2019.

[3] A. Thieuw and H. Marcille. Pleiades-HR CMGs-based attitude control system design, development status and performances. *IFAC Proceedings Volumes*, 40(7):834–839, 2007.

[4] M. Bernard, D. Decluseau, L. Gabet, and P. Nonin. 3d capabilities of pleiades satellite. *Int. Arch. Photogramm. Remote Sens. Spatial Inf. Sci*, 39:B3, 2012

[5] A.M. Elbeltagy, A. Youssef, A. Bayoumy Aly, and Y. Elhalwagy. Fixed ground-target tracking control of satellites using a nonlinear model predictive control. *Mathematical Modelling of Engineering Problems*, 5(1):11–20, 2018.

[6] F. Chaumette and S. Hutchinson. Visual servo control, Part I: Basic approaches. *IEEE Robotics and Automation Magazine*, 13(4):82–90, December 2006.

[7] A. Petit, E. Marchand, and K. Kanani. Vision-based space autonomous rendezvous : A case study. In *IEEE/RSJ Int. Conf. on Intelligent Robots and Systems, IROS'11*, pages 619–624, San Francisco, USA, September 2011.

[8] H. Wang, D. Guo, H. Xu, W. Chen, T. Liu, and K.K. Leang. Eye-in-hand tracking control of a free-floating space manipulator. *IEEE Trans. on Aerospace and Electronic Systems*, 53(4):1855–1865, 2017.

[9] J.P. Alepuz, M. R. Emami, and J. Pomares. Direct image-based visual servoing of free-floating space manipulators. *Aerospace Science and Technology*, 55:1–9, 2016.

[10] A.H. Abdul Hafez, P. Mithun, V.V. Anurag, S.V. Shah, and K. Madhava Krishna. Reactionless visual servoing of a multi-arm space robot combined with other manipulation tasks. *Robotics and Autonomous Systems*, 91:1–10, 2017.

[11] P. Mithun, H. Pandya, A. Gaud, S. V Shah, and K. M. Krishna. Image based visual servoing for tumbling objects. In *IEEE/RSJ Int. Conf. on Intelligent Robots and Systems*, pages 2901–2908, 2018.

[12] K. Hashimoto and H. Kimura. Visual servoing with non linear observer. In *Proc. IEEE Int. Conf. on Robotics and Automation, ICRA'95*, pages 484–489, Nagoya, 1995.

[13] A. Crétual and F. Chaumette. Dynamic stabilization of a pan and tilt camera for sub-marine image visualization. *Computer Vision and Image Understanding*, 79(1):47–65, July 2000.

[14] H. Wang, Y. Liu, W. Chen, and Z. Wang. A new approach to dynamic eye-in-hand visual tracking using nonlinear observers. *IEEE/ASME Trans. on Mechatronics*, 16(2):387–394, 2010.

[15] F. Chaumette and S. Hutchinson. Visual servo control, Part II: Advanced approaches. *IEEE Robotics and Automation Magazine*, 14(1):109–118, March 2007.

[16] M. Robic, R. Fraisse, E. Marchand, F. Chaumette. Vision-based rotational control of an agile observation satellite. In *IEEE/RSJ Int. Conf. on Intelligent Robots and Systems, IROS'22*, Kyoto, Japan, Octobre 2022.

[17] E. Marchand, F. Spindler, and F. Chaumette. ViSP for visual servoing: a generic software platform with a wide class of robot control skills. *IEEE Robotics and Automation Magazine*, 12(4):40–52, December 2005.

[18] S. Baker and I. Matthews. Lucas-Kanade 20 years on: A unifying framework. *Int. Journal of Computer Vision*, 56(3):221–255, 2004.